Terrain Relative Navigation for Guided Descent on Titan

Larry Matthies, Shreyansh Daftry, Brandon Rothrock, Anthony Davis, Robert Hewitt, Evgeniy Sklyanskiy, Jeff Delaune, Aaron Schutte, Marco Quadrelli, and Michael Malaska
Jet Propulsion Laboratory, California Institute of Technology, USA
Email: lhm@jpl.nasa.gov

Joshua Yurtsever
Department of Electrical Engineering and Computer Sciences
University of California Berkeley, USA

***Abstract*—Titan's dense atmosphere, low gravity, and high winds at high altitudes create descent times of >90 minutes with standard entry/descent/landing (EDL) architectures and result in large unguided landing ellipses, with 99% values of ∼110x110 km and 149x72 km in recent Titan lander proposals. Enabling precision landing on Titan could increase science return for the types of missions proposed to date and make additional types of landing sites accessible, opening up new possibilities for science investigations. Precision landing on Titan has unique challenges, because the hazy atmosphere makes it difficult to see the surface and because it requires guided descent with divert ranges that are one to two orders of magnitude larger than needed for other target bodies, i.e. up to on the order of 100 km. It is conceivable that such a divert capability could be provided economically by a parafoil or other steerable aerodynamic decelerator deployed several 10s of km above the surface. The long descent times lead to large inertial navigation errors, hence a need for terrain relative navigation (TRN). This would require a TRN capability that can operate at such altitudes, despite challenges of seeing the surface sufficiently clearly and of depending on map products that are two orders of magnitude lower in spatial resolution than those for Mars and airless bodies.**

This paper addressed the TRN problem for Titan guided descent, assuming parafoil deployment at an altitude around 40 km. We define a notional sensor suite including an inertial measurement unit (IMU), a radar altimeter, and two descent cameras, with spectral responses in the visible/near infrared (VNIR) (∼0.5 to 1 um) and short wave infrared (SWIR) (∼2.0 to 2.1 um). Due to the low resolution of current Titan map products, we define two altitude regimes (above and below ∼20 km) that need different navigation techniques. Map matching is applicable in the upper regime, but challenging or infeasible in the lower one. Feature tracking with decent imagery is desirable in the lower regime, but challenging in the upper one. We derive image contrast requirements for TRN from prior literature and create models of achievable image contrast by radiative transfer modeling; this shows that the requirements should be achievable for a SWIR descent camera in the upper regime, and that a VNIR descent camera is preferable in the lower regime.

We then develop algorithms for map matching and feature tracking with descent images and test these with synthetic images created from Cassini/Huygens data sets and our radiative transfer model. We also introduce new possibilities for TRN based on the potential to discriminate some specific types of terrain onboard in descent imagery, such as lake vs adjacent ground and dune vs interdune. We use sensor measurement noise models in simulations of state estimation with an extended Kalman filter that includes coordinates of a set of tracked features in the state vector. Case studies were done for two notional landing sites, one in a site with only dry ground and one in a Titan lake district. In both cases, the filter error model shows 3σ position error at touchdown on the order of 2 km. More work is needed to validate these results with higher fidelity camera models and larger data sets, but this is very promising.

The research described in this paper was carried out at the Jet Propulsion Laboratory, California Institute of Technology, under a contract with the National Aeronautics and Space Administration.
978-1-7281-2734-7/20/$31.00 ©2020 IEEE

TABLE OF CONTENTS

1. INTRODUCTION

The Titan Huygens probe and other Titan probe/lander mission proposals to date have had large 99% landing error ellipses: at least 405x52 km for Huygens [1], ∼110x110 km for TiME [2], and ∼149x72 km for Dragonfly [3]. The major axis of the Huygens ellipse was especially large because that mission was designed for a long descent time for atmospheric science and descent imaging. Aside from that, it is difficult to get Titan landing precision much below these ellipse sizes with unguided entry, descent, and landing (EDL) systems. This limits choices of landing sites to regions that are expected to be free of landing hazards over comparable areas, such as large plains, seas, or dune fields. This in turn limits options for science objectives. With such ellipses, mission concepts with *in situ* mobility systems that have key science targets outside the landing ellipse may require traverses exceeding 100 km and several months of mission operations after landing to reach such targets.

As has been the case for Mars, enabling more precise landing on Titan would allow placing landing ellipses in locations with smaller hazard-free areas and delivering *in situ* mobility systems closer to their ultimate destinations. This could include landing near the edge of a dune field, near the shore of a sea, or in small lakes. With further work on landing hazard analysis, hazard tolerance, or hazard avoidance, it could also enable landing in or near potential cryovolcanic regions, icy mountain terrain, dry lakebeds, and other features of interest [4].

Titan's dense, tall, hazy atmosphere makes precision landing a different and more difficult problem for Titan than for Mars and airless bodies. The atmosphere limits the spectral bands in which Titan's surface can be seen from orbit and limits the spatial resolution of orbital remote sensing imagery.

Titan map products from the Cassini mission have pixel sizes ranging from ∼300 m to ∼3 km [5], [6], compared to <1 m/pixel for Mars and airless bodies [7]. The current paradigm for obtaining position knowledge during descent for precision landing is to use a style of terrain relative navigation (TRN) that does real-time, onboard registration of descent images to maps that were created from prior orbital reconnaissance images [7]. This limits the precision of position knowledge during descent to something comparable to the map pixel size, which means kilometer-scale position uncertainty for Titan, compared to 10s of meters for Mars. For Mars, most of the lander delivery error is removed by guided entry. Control authority for divert during descent is provided by a rocket propulsion system, with a maximum divert range limited by fuel load to a few hundred meters or at most a few kilometers [8]. On Titan, atmospheric entry flight path angles can be far steeper than for Mars (e.g. >50 degrees vs <15 degrees); this limits the need for guided entry, because dispersion grows relatively little during a steep entry. Conversely, descent is far longer on Titan than on Mars (>90 minutes vs ∼4 minutes). Therefore, on Titan the bulk of lander delivery error accrues during descent, and descent guidance with large divert capability is required for precision landing [2].

On Earth, low-cost precision aerial delivery systems (PADS) use guided parafoils with GPS-based navigation to achieve delivery errors of <100 meters when good wind knowledge is available [9], [10], [11]. Results from the Huygens probe indicated that Titan's surface became visible in descent images at around 40 km above ground level (AGL) [12]. If a guided parafoil with a moderate glide ratio of $\sim 3:1$ could be used from that altitude, with TRN for navigation, this might enable glide ranges sufficient to reach any point in the lander delivery ellipses of recent proposals, potentially with kilometer-scale delivery error.

NASA recently funded a low to mid-TRL study of this concept under the COLDTech program. This paper reports results from that study on the TRN part of the problem. The following section expands on related prior work. Section 3 describes notional mission scenarios that motivated this work and notional landing sites that were selected as case studies. Section 4 provides an overview of our approach to TRN on Titan, which serves as a more detailed introduction to subsequent discussions on camera modeling (section 5), map matching (section 6), feature tracking (section 7), segmentation (section 8), and multi-sensor state estimation (section 9). Section 10 summarizes our main conclusions and lists key areas for future work.

2. Background and Related Work

Terrain relative navigation capabilities for precision guidance of cruise missiles began with development of the Digital Scene Matching Area Correlation (DSMAC) system in the 1970s [13], [14]. Precision landing capabilities for planetary exploration have been studied at least since work in the 1980s on a Mars Rover Sample Return (MRSR) mission concept of that era [15]. Work on precision landing accelerated in 2005 when it became the focus of the Space Technology 9 (ST-9) mission of NASA's New Millennium Program [16], [17]. Work continued in the last two decades with a focus on the moon under the ALHAT program [18], [19] and a focus on Mars through development of precision guided descent capability for the 2020 Mars rover mission (M2020) [7]. Ongoing work has been extending this capability for precision landing on Europa [20].

The Lander Vision System (LVS) for M2020 [7], [21] is representative of the current state of the art in map-relative localization for TRN. Orbital reconnaissance imagery of Mars is available with a resolution of ∼30 cm/pixel from the HiRISE camera; this is processed into maps at two resolutions, 12 and 6 m/pixel, for coarse and fine localization processes, respectively. Map-relative localization uses onboard altitude and attitude knowledge to project descent images onto the ground plane and to resample them with the orientation and pixel scale of the prior map. The resampled descent images are then registered to the map using traditional template matching techniques that conduct a 2-D search for the best match position. The orbital and descent cameras have similar spectral responses and lighting conditions, so template matching uses simple algorithms based on normalized cross correlation (NCC). This processing pipeline is implemented in a field programmable gate array (FPGA) coprocessor to provide the necessary low latency output.

LVS includes two matching modes [21]. In coarse matching mode, descent image templates of 128x128 pixels are correlated against 1024x1024 search windows in the map using a frequency domain correlator implementation. In fine matching mode, 15x15 pixel templates from descent images are matched in 100x100 pixel map search windows using a spatial domain correlator implementation. LVS achieves a position error <40 m relative to the map. As we discuss below, the approach we developed for Titan is similar in important respects to the fine matching mode of LVS, though necessarily with far greater position error.

Guided parafoils with GPS-based navigation are now fielded for PADS in military and other applications, with delivery error that can be <100 m [9], [10], [11]. Glide ratios of around 3:1 are common, and 4:1 to 5:1 are available in systems for human skydivers [22]. Steerable parachutes have been studied for potential use in EDL architectures for pinpoint landing on Mars, but work to date has not shown sufficient benefit to include them [23]. The potential value of a guided parafoil for Titan was noted in [2], but not explored in detail.

3. Mission Scenarios

Science Objectives and Candidate Landing Sites

This project sought to be relevant to medium-cost missions (e.g. New Frontiers) starting with the next conceivable flight opportunity. Therefore, the project assumed no new orbital reconnaissance beyond that produced by the Cassini mission, no communication relay asset for a lander (i.e. direct to Earth communication), and launch opportunities roughly in the 2030s. This implies Titan arrival between the late 2030s through the 2040s. With Titan's northern spring equinox in 2039, this led to focusing on landing site scenarios from low latitudes up to high northern hemisphere latitudes.

Broad categories of high priority science questions for the surface of Titan include understanding its geology, the composition of its solid surface and its lakes and seas, its methane cycle, which includes potential subsurface transport of liquids, and its habitability, which includes the potential for interaction of surface organics with liquid water [25]. These questions can be addressed by future missions to Titans plains, dunes, lakes/seas, water-ice rich mountains, impact craters that could have had transient water melts, and locations where the subsurface ocean may have broached the surface (putative cryovolcanic areas) [4]. These terrain types

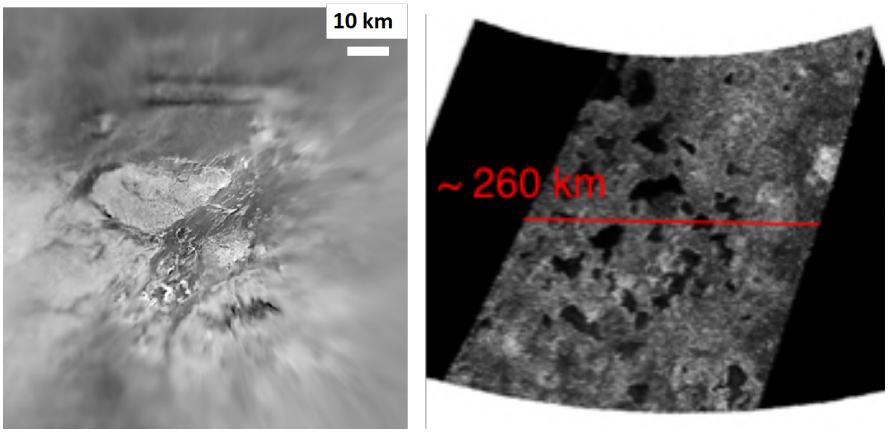

Figure 1. Left: Nested mosaic of descent imagery of the Huygens landing site, from the Descent Imager/Spectral Radiometer (DISR) instrument [24]. Right: Maracaibo Lacus region from a synthetic aperture radar image mosaic

can be addressed by different classes of progressively greater divert range and guidance and control (G&C) capability, which in principle could be served by different steerable parachute systems. These classes include:

- Relatively short diverts (e.g. <5 km) to land on interdune areas of dune fields
- Medium-range diverts (e.g. <50 km) to reach one of several acceptable landing sites spread throughout the ellipse or to land near seashores trending parallel to the landing ellipse major axis
- Large diverts (e.g. 50 to 100 km) to reach any point in a landing ellipse

Our main focus is the last class, but this work is relevant to all three classes. As case studies for this project, two notional landing sites (Figure 1) were selected that span a broad range of scientific, technological, and mission design issues and that have among the best available remote sensing imagery for developing algorithms and validating performance models. Both sites fall in the medium to large divert classes defined above:

- The Huygens probe landing site (10.25°S, 192.32°W) is a low latitude site, representing scientific interest in geology and surface composition, where descent imagery would view only dry ground. It has among the best orbital mapping coverage and the only descent imagery available for Titan, which makes it very useful for testing TRN algorithms for any dry ground landing site.
- The Maracaibo Lacus interlake region (74.95°N, 128.67°W) is a high northern latitude site, representing scientific interest in lake composition, lake formation processes, and potential subsurface methane transport. A mission scenario with *in situ* mobility here could visit and sample multiple lakes, including lakes on either side of a drainage divide. Descent imagery would contain a mixture of lakes and dry ground, which enables developing and testing TRN and G&C algorithms to address issues this raises. This location has good mapping coverage from all Cassini instruments; in particular, synthetic aperture radar (SAR) image mosaics have potential advantages in this kind of terrain (Section 8).

Entry, Descent, and Landing Architecture

To set a system context within which to study TRN, we defined a notional EDL architecture with the following key characteristics (Figure 2):

- Late release of the entry system from the cruise stage, to maximize the accuracy and precision of delivery and state knowledge at atmospheric entry, analogous to the Mars Science Laboratory (MSL) mission [8].
- An unguided entry phase, followed by rapid descent with a small drogue parachute (or possibly no drogue parachute [26]) to an altitude where guided descent can begin.
- Deployment of a larger drogue for heat shield separation, which allows a radar altimeter and a descent camera to begin operation, which enables initializing the TRN system and generating improved position, velocity, and yaw knowledge.
- Release of the lander from the backshell, which deploys the parafoil.

After selecting the best reachable landing site target, if more than one acceptable candidate is defined in the mission concept, parafoil operations follow a typical sequence of phases [27]:

- "Homing", which includes the initial turn toward the target followed by a fairly direct glide to the vicinity of the target.
- "Energy management", which is a series turns to reduce altitude while loitering near the target, culminating at a low-altitude waypoint downwind of the target.
- "Final approach", which turns upwind and glides toward the target to minimize ground speed.
- "Flare", which is a pitch maneuver to reduce horizontal and vertical velocity just before touchdown.

Parafoil sizing studies suggest that the total parafoil descent time from 40 km AGL would be 3 to 4 hours. The parafoil operation phases above have implications for a TRN system,

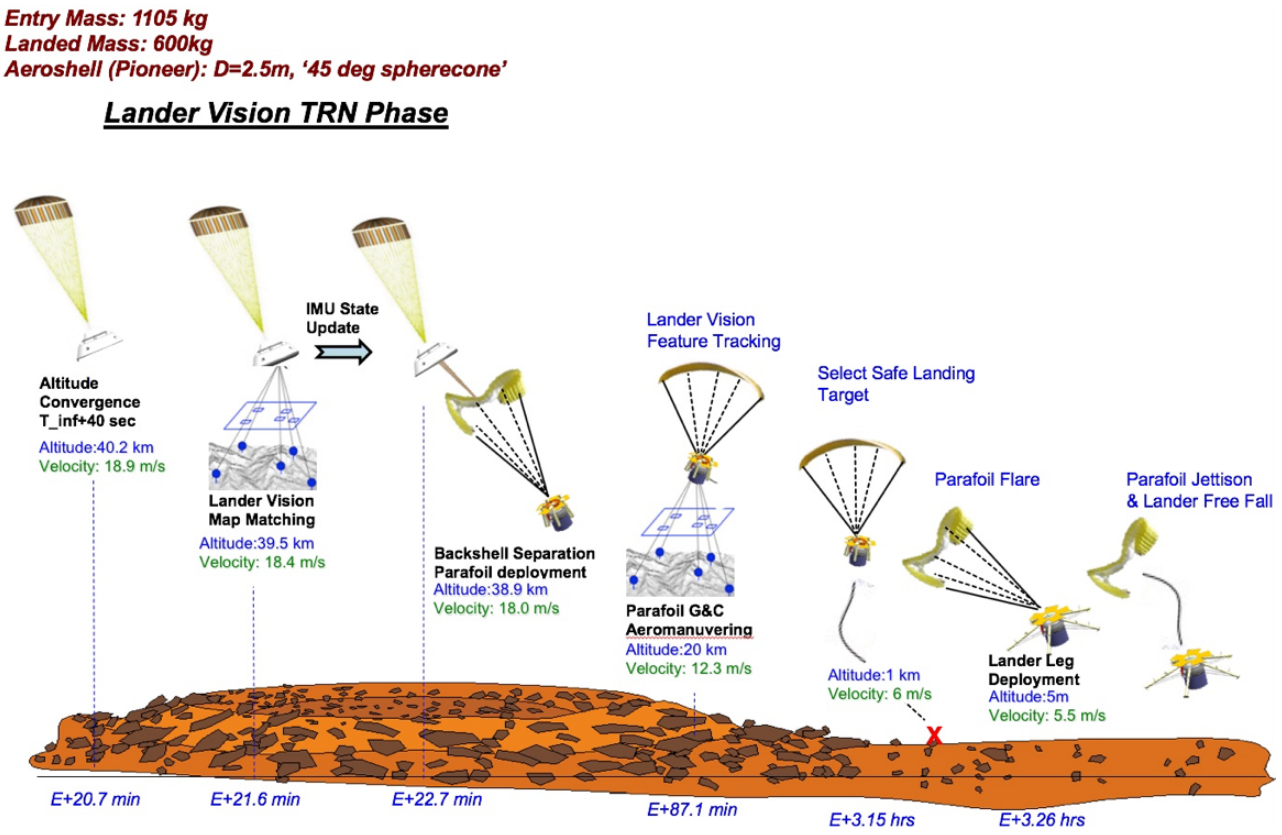

Figure 2. EDL conops from TRN initialization until touchdown.

as discussed below. The balance of this paper addresses TRN. Aspects of parafoil dynamics, guidance, and control, as well as an integrated simulation environment developed to develop and test guidance, navigation, and control algorithms in this context, are discussed in [28].

4. Terrain Relative Navigation Overview

This section discusses available map products, our notional TRN sensor suite, altitude regimes that have distinct requirements, and required TRN algorithms.

Map Products

Without new orbital reconnaissance, map product options are mosaics produced with data from the three mapping instruments on the Cassini Orbiter:

- A NIR band $\sim$10 nm wide centered at 938 nm, acquired by the ISS camera. The best mosaic of this data is sampled with a spatial resolution of about 3 km/pixel [6].
- A SWIR band from $\sim$2.0 to 2.1 um, acquired by the VIMS instrument. The best VIMS image resolution is $\sim$1 km/pixel, but most is much lower resolution [29].
- SAR image mosaics, with best resolution of $\sim$300 m/pixel [5].

The NIR mosaic has the best global coverage and better signal-to-noise ratio (SNR) than the SWIR mosaic. The SAR mosaic has much higher resolution for some locations, which makes it an attractive candidate for those locations. For reasons noted in Section 6, our experience to date indicates that the NIR mosaic is the best candidate for dry ground sites and the SAR mosaic is very promising for lake district sites.

Notional TRN Suite

We assume good state knowledge initialization from the cruise stage at entry minus 10 minutes (E-10), as was done for MSL [8]. A navigation-grade IMU is required for inertial propagation of state knowledge; we assume performance equivalent to the MIMU used for MSL. Altimetry is required in the EDL architecture after heat shield separation, which may occur at an altitude of several 10s of km. Performance of the radar altimeter used by the Huygens probe was taken as representative for this, which had a final design goal for operation up to 60 km AGL with $<5\%$ error [30].

Atmospheric light absorption and scattering limit the options for spectral response of descent cameras to a VNIR band similar to the DISR cameras, which was 660 to 1000 nm, and the SWIR band of the VIMS mosaic mentioned above. These have sufficiently different potential performance characteristics that we studied both, assuming that cameras were nadir-pointed with a field of view (FOV) of 90x90 degrees and f/2 optics, which is similar to the LVS system [7].

Altitude Regimes

Reliability of map matching is poor if descent images subtend a very small number of map pixels. Given the assumed descent camera FOV and the resolution of the Titan map

products, this implies that map matching must operate above some minimum altitude, which is likely to be $\sim$10 to 20 km AGL. Atmospheric scattering reduces the contrast of descent imagery as altitude increases, which places an upper bound on feasible altitudes for map matching. Below the cut-off altitude for map matching, parafoil descent will take 1 to 2 hours, during which position estimation error will grow unacceptably if only IMU and altimeter sensors are used. Therefore, some form of terrain-relative sensing is still required. Suitably small radar and lidar velocimeters are not currently available for this whole altitude range. Tracking descent image features between images acquired at different altitudes potentially enables estimating position displacements between such images. Several variations on this theme are possible, but we refer to them here as a class that we call feature tracking. In principle, feature tracking may also be used above the map-matching cut-off altitude.

So far, we have two altitude regimes to consider: an upper regime with map matching and optional feature tracking, and a lower regime with only feature tracking. For initial study, we took 40 to 20 km as nominal bounds for the upper regime and 20 km to touchdown as nominal bounds for the lower regime. Parafoil flare maneuvers must be timed very well to be effective, which needs very accurate altitude and velocity knowledge. This could define a third regime very close to the ground, for example where a second altimeter with a much different dynamic range may be useful; this is out of scope here.

Required TRN Algorithms

Three classes of algorithm require study based on the discussion above: map matching, feature tracking, and multi-sensor state estimation algorithms that can fuse all of the sensor measurements. These are all analogous to functionality that has been studied for TRN on Mars and Europa [21], [20], though details will differ for the Titan environment. Another class of algorithm is relevant, because Titan has a few specific classes of terrain that may be recognizable directly in descent imagery. Titan's methane lakes absorb light very strongly, especially in the SWIR band. Therefore, when viewed away from a reflection of the sun, the reflectivity contrast between lake and adjacent ground is likely to make it possible to discriminate these terrain types automatically in descent images. In dune fields, dune and interdune regions often have predictably different albedos and will have different shading that is a function of sun angle. This may make it possible to discriminate these regions in descent imagery. This discrimination process falls under the general class of algorithms called image segmentation. If this is done successfully, guidance and navigation may be possible relative to the terrain types identified in this way, without necessarily referencing a prior map; in particular, this may be useful in the lower altitude regime where current map matching techniques are inapplicable.

Since the performance of descent image processing algorithms depends critically on the quality of those images, and since that quality is a strong function altitude and spectral band, the next section addresses this issue. Following sections address the four classes of algorithm listed above.

5. Modeling Descent Cameras and Image Quality

Key characteristics of descent cameras and descent image quality to examine are (1) which spectral bands to use for which vision functions, over what ranges of altitudes, (2) what image spatial resolution, signal-to-noise ratio (SNR) and contrast is required and/or achievable, and (3) how potential for image smear due to camera motion affects the camera specifications.

The low resolution of Titan map products implies a large amount of binning of descent images for map matching [21], which significantly helps meet image smear and SNR requirements. Linear camera motion does not cause appreciable smear at altitudes germane here, but camera rotational velocity requires analysis. Camera rotation primarily is caused by lander attitude dynamics, influenced by disturbances and by how the lander is attached to the parachute. The Huygens probe was attached with a single point swivel; RMS swing rates were estimated approximately as $<$5 deg/sec below 5 km, $<$7 deg/sec below 10 km, $<$10 deg/sec below 20 km, and $<$20 deg/sec below 40 km [24]. Payloads have been attached to parafoils with 1, 2, or 4-point rigging [26]. Here we assume 4-point rigging, which makes the parafoil plus lander system approximately a rigid body. In that case, the main component of rotation is due to parafoil turn maneuvers, which are generally $<$10 deg/sec [31]. We used that upper bound, rounded to 0.2 rad/sec. For maps with 3 km/pixel, at 40 km above ground level (AGL) descent images with 90x90 deg FOV will be binned to approximately 27x27 pixels. A half-pixel smear constraint in these conditions allows image exposure up to about 93 ms.

A useful image quality metric for map matching and feature tracking algorithms is the dynamic range of image intensities relative to the average image noise level, or contrast SNR (CSNR). Light scattering in Titan's hazy atmosphere reduces the contrast of descent images progressively with increasing altitude. This requires defining CSNR in terms of the dynamic range of unscattered light that reaches the camera from Titan's surface (direct), ratioed with the noise level of the average image exposure, which includes the scattered light. CSNR is also useful as a simple predictor of the feasibility of segmenting descent imagery into two different terrain types with different albedos, such as dune vs interdune or lake vs ground.

We estimate the required CSNR by examining results from processing descent imagery from the DISR descent cameras on the Huygens probe [24] and from testing the LVS system [7]. Features typically were sufficiently apparent in DISR images from altitudes below 30 km for tie-points to be manually matched. An RMS estimate of image contrast at that altitude was about $+/-0.2\%$ from the mean value in small image regions, i.e. a full range of 0.4% (1 DN in 8-bit images). Typical image exposures were about 1/3 of full range and had SNR of $\sim$200 ($\sim$0.4 DN). This yields a CSNR estimate of 2.5. The fine matching mode in LVS is a reasonable analog to map matching and feature tracking here [21], which may use template sizes ranging from $\sim$2x larger to $\sim$2x smaller than LVS with smaller search regions than LVS ($\sim$30x30 pixels). In simulation-based stress testing of the entire LVS system, success was achieved with descent image contrasts as low as 4 DN for 8-bit images, with an image noise level equivalent to 1.6 DN. This is also a CSNR of 2.5. Therefore, we take this as a rough lower bound requirement.

Considering the two spectral bands that are plausible for descent imagery (VNIR and SWIR), the VNIR band has more light available than the SWIR band, but is more affected by scattering. The scattering effect dominates CSNR at high altitudes, favoring the use of SWIR imagery; the overall light

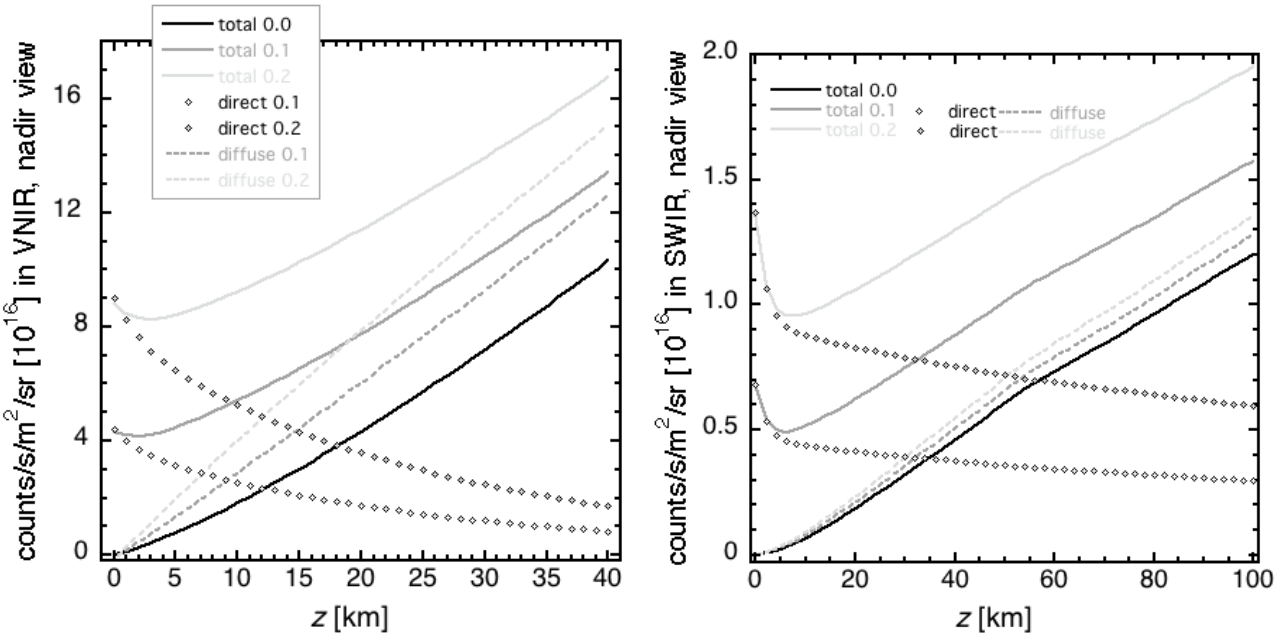

Figure 3. Elements of total radiance (direct, diffuse, total) at the sensor vs. altitude. Left: VNIR spectrum. Right: SWIR spectrum (range extended from 40 to 100 km.

level dominates at low altitudes, favoring the use of VNIR imagery. To quantify this, we used the DISORT radiative transfer code [32] to model light absorption and scattering from the top of the atmosphere, to the surface, and into the camera, assuming Lambertian surface reflectance. Aerosol distributions and scattering properties for this were obtained from [33]; methane abundance profiles were obtained from [34]. As notional models for descent camera performance, we used specifications of the H1RG image detector for the SWIR band, which was used in the Titan AVIATR study [35], and the CMV20000 image detector for the VNIR band, which was a candidate Mars descent camera when this study began. The H1RG has 1024x1024 pixels with a well depth of 80,000 electrons (e-) and a quantum efficient (QE) at 2 um of $>70\%$. The CMV20000 has 5120x3840 pixels, a well depth of 15,000e-, and a peak QE of $\sim 40\%$ at around 550 nm. For Mars applications, the CMV20000 is binned in firmware to resolutions of 1024x1024 pixels or less. We assume that filters limit the spectral response of these cameras to appropriate bands. We did not attempt to optimize the bands, but assumed 2.0 to 2.1 um for SWIR and 500 to 1000 nm for VNIR. The assumptions of f/2 optics and 90x90 degree FOV were used to determine aperture areas of 16.7 mm^2 for the notional SWIR camera and 29.6 mm^2 for the notional VNIR camera.

Surface albedos of 0.1 and 0.2 were used with DISORT to compute radiance from Titans surface as a function of altitude for direct (unscattered) and diffuse (scattered) light, in units of electrons/m^2/sr/nm, i.e. weighted by detector QE (Figure 3). The amount of direct light drops with increasing altitude, whereas scattered light increases rapidly with altitude. Data points from these curves are multiplied by aperture area, pixel IFOV, and image exposure time to determine pixel exposure levels in electrons.

Estimating CSNR requires a model of surface reflectively variation. RMS values of $\sim 5\%$ have been estimated for the Huygens landing site in the VNIR band of the DISR cameras [36]. We use this as a nominal value for both VNIR and SWIR; higher values exist at other locations, e.g. dune fields [37] and lake districts (section 8). We assume that binning is done by digitizing to 8, 10, or 12 bits per pixel, then averaging b*b pixels for a value of b that is determined by the initial image resolution, map resolution, altitude, and FOV. Binning improves CSNR by somewhat less than a factor of b, since A/D conversion adds quantization noise.

At 40 km AGL, for a 3 km/pixel map mosaic, a 90x90 deg FOV descent camera sees $\sim$27x27 map pixels. For the notional SWIR camera, this implies a binning factor of 40 and a smear-free exposure time of $\sim$93 ms for 0.2 rad/sec turns. With this, the model above predicts a CSNR of 158, which is far greater than needed for map matching. Feature tracking is not necessarily required when map matching is possible, but it can help with heading estimation, especially when map resolution is low. There is some freedom to choose the image resolution used for feature tracking, based on CSNR and other factors, but for applications on Earth this is generally 512x512 pixels or greater. To achieve a CSNR of 2.5 at this resolution for the SWIR model, camera rotations must be limited to $\sim$2 deg/sec. This is plausible in the parafoil homing phase, when the system is flying an approximately steady heading toward the landing site, but more analysis of attitude dynamics of the entire parafoil system is required to make a stronger statement. The notional VNIR camera would have adequate CSNR for map matching at this altitude due to the very large binning factor, though much lower than the notional SWIR camera. However, CSNR with a VNIR camera would be inadequate for feature tracking in this altitude regime.

Assuming that map matching stops at around 20 km AGL, feature tracking is essential below 20 km to limit the growth of heading estimation error. Parafoil turns are more likely to

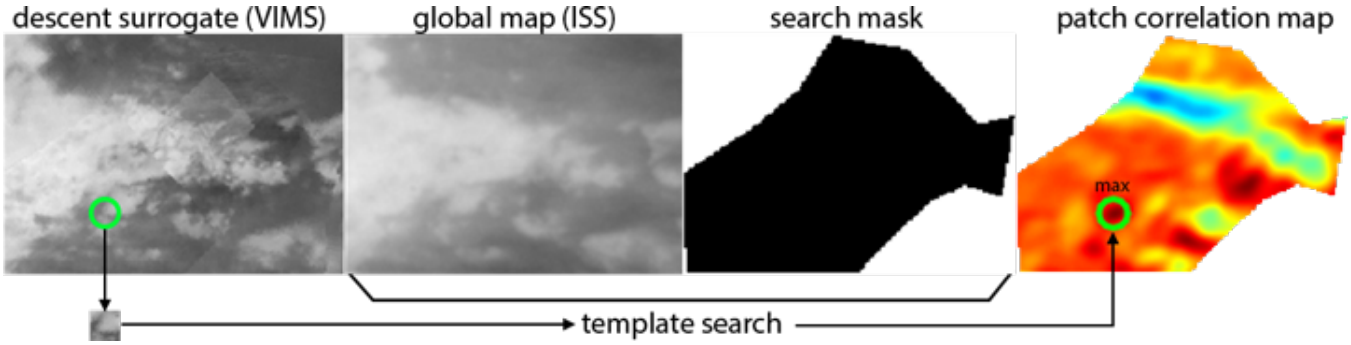

Figure 4. Illustrations of the process for map matching experiments for the Huygens site with an ISS map mosaic. Left to right: (1) VIMS mosaic used to create simulated descent images; green circle and image patch below it represent one simulated descent image chosen randomly from the mosaic. (2) ISS map mosaic. (3) Region of the two mosaics used for experiments to avoid mosaicking artifacts. (4) False color rendering of similarity scores from the matcher, showing where the simulated descent image best matches the map mosaic; dark blue is best, red is worst. Many trials were run with different random selections of descent image template from the VIMS mosaic.

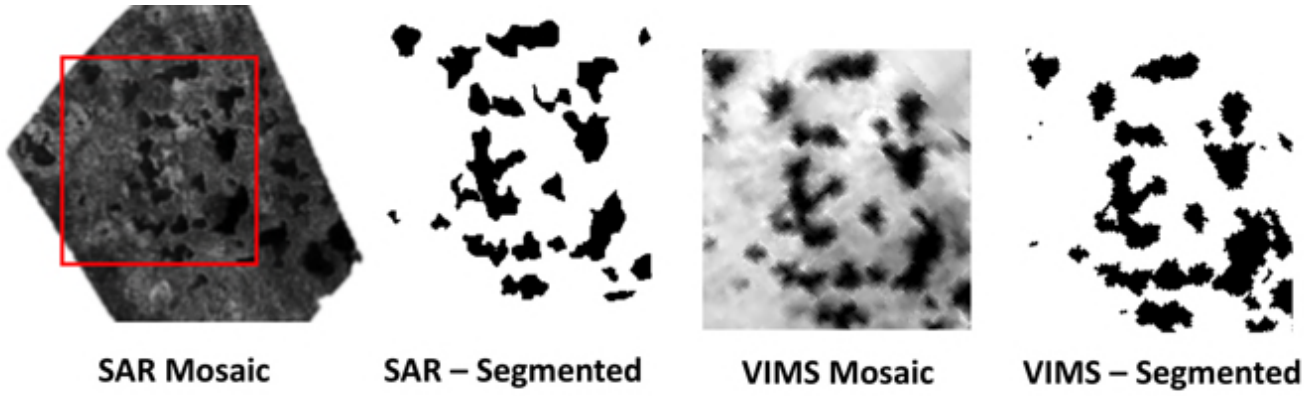

Figure 5. Illustrations of the process for map matching experiments for the Maracaibo Lacus site with a SAR map mosaic. Left to right: (1) SAR mosaic, with red rectangle showing an area cropped for experiments. (2) Binarized SAR mosaic, where black pixels lie on lakes and white pixels lie on dry ground. (3) VIMS mosaic of the same area, used to create simulated descent images. (4) Binarized VIMS mosaic. The process for repeated experiments was the same as for the top row.

occur as altitude reduces in order to remain near the target; therefore, in this regime we apply the smear-free requirement for 0.2 rad/sec turns to image resolutions required for feature tracking. This leads to short exposure time limits that imply that the SWIR camera cannot achieve adequate CSNR. For VNIR, with much more light available, our model predicts a CSNR of ∼3.7. CSNR will improve with decreasing altitude, since direct light from the surface increases (less attenuation) and the effects of scattering decrease; this will continue to favor the use of VNIR for feature tracking.

This analysis supports conclusions that map matching with SWIR descent imagery is feasible for altitudes of at least 40 km, and will yield better CSNR than VNIR descent imagery. Feature tracking is plausible with SWIR imagery at 40 km AGL if camera rotation rates are less than a few degrees/sec, but likely to be impractical with VNIR. Our nominal cut-off altitude for map matching is 20 km, based on the size of map pixels; this value could change with more work on algorithm design and testing. Feature tracking below 20 km AGL is better with VNIR than with SWIR descent imagery.

6. Multi-modal Map Matching

Algorithm

Map matching techniques for TRN generally simplify the registration problem by using altitude and attitude knowledge to project descent images onto the ground plane, then resample the descent images at the resolution of the map. The work here assumed that such projection and resampling was done, but did not model error in altitude and attitude knowledge. This converts the registration problem into a 2-D search for the best match location in ground (X-Y) coordinates. This approach has potential to apply to any landing site on Titan where the orbital imaging is adequate.

For landing scenarios on dry ground, the map matching problem translates to registering SWIR descent images to Titan map products created from ISS, VIMS or radar data. The best global mosaics are available from ISS; the best spatial resolution is available for selected locations from radar. Since the spectral bands for SWIR do not overlap with either ISS or radar, this is a multi-modal image registration problem. While many approaches for 2-D image registration exist in

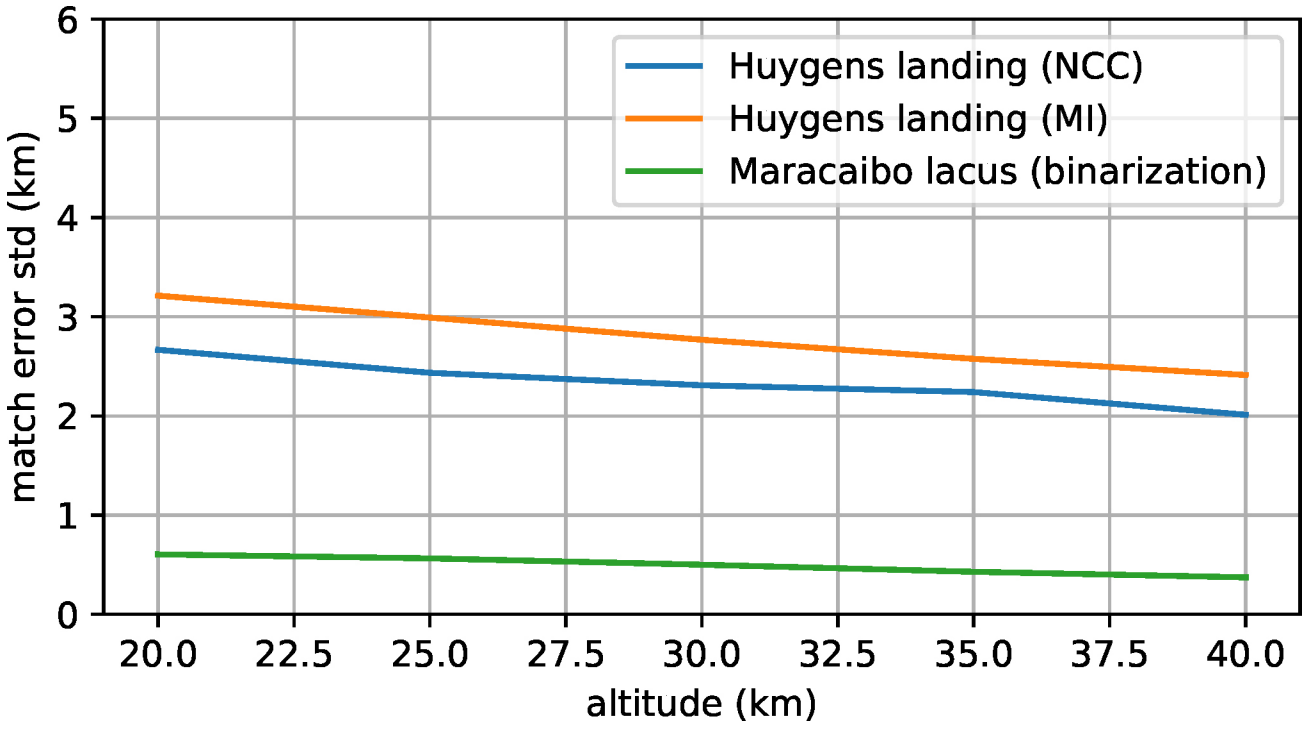

Figure 6. 1σ map matching errors for 1000 trials at every $5km$ of altitude. Errors increase at lower altitudes because of the fixed, low resolution of the map.

general [38], [39], the majority assume similarity in the underlying image intensities at corresponding pixels, possibly modulo some easily modeled transformation. In cases where registration is required between sensors capturing different physical phenomena, the majority of these techniques fail. Furthermore, the hazy atmosphere and relatively low image contrast at Titan suggested that registration methods based on template matching may be more successful than methods based on matching distinctive keypoints [40]; therefore, we examined the former.

Classic template matching methods using normalized cross correlation (NCC) have been used successfully in the past for image-registration problems for applications on Mars [7]. However, it was unclear if this would for our Titan scenario. Much more computationally expensive methods, such as the mutual information (MI) similarity score, have been used successfully for registering multi-modal medical imaging and Earth remote sensing data sets, and have shown some success in prior work with Titan data sets [41], [42]. In this work, we evaluated the performance of both NCC and MI with data from the Huygens site. For experiments with NCC, we also perform sub-pixel matching [43].

Regions of small lakes in northern latitudes such as Maracaibo are an interesting scenario for map matching algorithms, because they offer the highest image contrast (between lake and ground regions) available on Titan. Liquid methane absorbs the radar and SWIR wavelengths so strongly that it is plausible to binarize both the map mosaic (done on Earth with human supervision) and the descent imagery (done automatically onboard) into lake versus non-lake pixels. This abstracts away differences in sensor phenomenology, and opens possibilities for a different approach to registration using a binary correlation algorithm [44] that is much simpler than MI or NCC. Studying segmentation algorithms for binarization was beyond our scope, so we binarized the map mosaic with an interactive image editing tool and used simple thresholding to binarize synthesized descent imagery.

Experiments

We used VIMS mosaics resampled at 2 km/pixel to generate simulated descent images, with ISS and radar data as the map (Figure 4, 5). We used the radiative transfer and camera models described in Section 5 to synthesize noisy descent images with a 90 degree FOV at a variety of altitudes. At several test altitudes, we created simulated descent images for many test locations to measure the mean and standard deviation of registration error (Figure 6). For the dry ground ellipse, NCC produced slightly lower error than MI; since NCC is much cheaper to compute and has flight heritage, this is a favorable result. Binary correlation worked well for the lake region, with lower error than the dry ground results because the SAR map has higher resolution than the ISS map. In general, error was lower at higher altitudes because descent images project to shrinking patches on the ground as altitude decreases, which produces noisier matches. Overall, 3σ error was around 1.5 km for the lake district using the SAR map and 8 km for the Huygens site using the ISS map. Filtering many measurements during descent reduces uncertainty further (Section 9).

7. Feature Tracking

Due to the minimum operating altitude for map matching (∼20 km), 2D feature tracking will be initiated at this altitude or higher on the VNIR camera generating a set of matches between successive images to be processed by the state estimation filter in addition to successful map matching measurements. Once map matching measurements are unavailable, the system will switch over entirely to visual-inertial odometry utilizing these feature matches. Because the performance of feature tracking is heavily dependent on image contrast, an analysis was done on the tracking performance from an altitude of 20 km AGL to landing using simulated imagery generated from the Huygens DISR descent imagery.

We modeled the VNIR descent camera after the EECAM [45] CMOS imager which will be used on the Mars 2020 mission. This includes a resolution of 3840x3840 binned down to 1280x1280 and a full electron well depth of 15,000 for each pixel. Assuming an image frame-rate of 5Hz, associated altitudes were generated from a simulated trajectory. An image sequence of the simulated descent was then created above the Huygens landing location. To do this, we started with the DISR descent imagery mosaic corrected for haze and viewing/emission angles such that the values in the mosaic are proportional to the surface *I/F* (radiance factor) [24] and scaled such that an image matching the altitude and region of image 450 in the Huygens image sequence approximately matches the contrast values reported in [46]. For each pixel in the simulated view a photon count was computed with haze re-added according to altitude, viewing angle, and the surface *I/F* values as presented in [47]. Random, zero-mean, approximately Poisson noise was then added to the photon count to simulate shot noise in the camera. Exposure time on the camera was adjusted such that the maximum brightness pixel was close to full, with a safety buffer to accommodate pixel shot noise. Examples of the resulting imagery and corresponding histograms in Figure 7 show how the contrast changes significantly with altitude due to the effect of Titan's haze.

The FAST corner detection algorithm [48] was used for feature detection in each image with a minimum contrast threshold of 1% between the corner and surrounding region. The features were then tracked in the next image using Lucas-Kanade-Tomasi tracking [49], [50], [51] with a window size of 7x7 pixels. The M-estimator SAmple Consensus algorithm [52] was then used to remove feature matches that didn't correspond to the consensus similarity transform between images. This was done on each sequential pair of frames throughout the trajectory and error statistics were computed to assess performance as a function of altitude throughout the trajectory.

The resulting error in matching is approximately zero-mean and Gaussian with the standard deviation plotted as a function of altitude in Figure 8. As expected, the error in tracking due to haze decreases throughout the descent as the contrast in the imagery improves. Note that from approximately 3 km AGL to landing, the tracking error standard deviation begins to rise. This is likely due to scale change between images becoming significant as well as the particular terrain in view at these altitudes (mostly the darker lowlands).

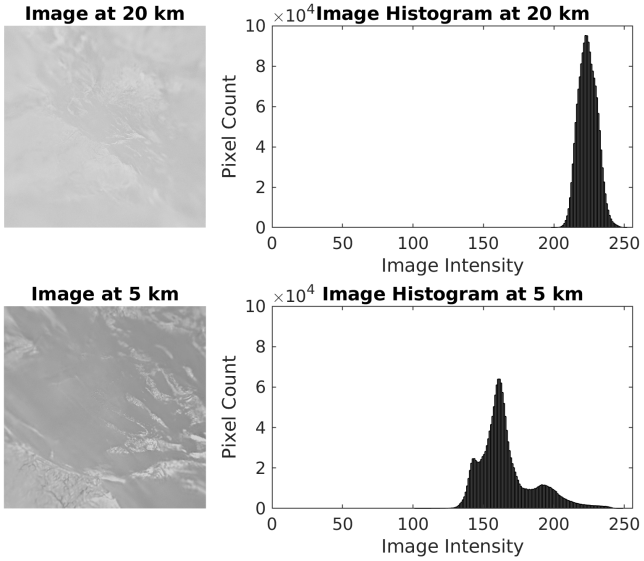

Figure 7. Example images generated at 20 and 5 km AGL from the DISR imaging mosaic and their respective histograms demonstrating the change in contrast with altitude due to Titan's haze.

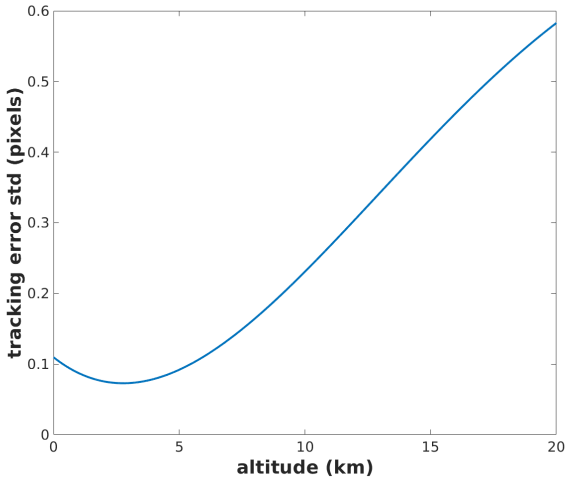

Figure 8. 1σ feature tracking errors from simulated images of the DISR imaging mosaic generated at 5 Hz.

8. Image-based Terrain Segmentation

In this section, we investigate the feasibility of automatic, onboard segmentation of scientifically interesting landmarks or science targets on Titan. Specifically, we look at the lakes vs dry ground scenario; such discrimination of landmarks in descent imagery could potentially provide very accurate estimates of descent vehicle position relative to these features, allowing access to scientifically interesting targets typically inaccessible with traditional map matching approaches.

For landing scenarios in the lake district, we model the appearance of lakes by estimating the total upwelling radiance. This is a combination of specular reflection from the lake surface, combined with reflection from the lake floor and

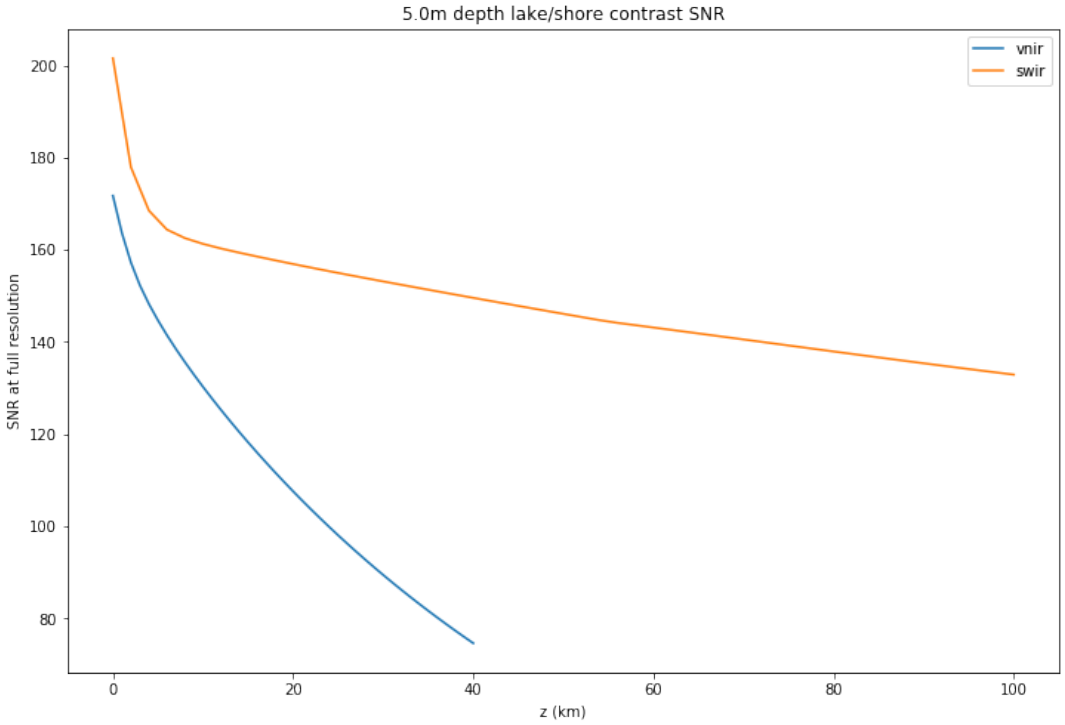

Figure 9. Contrast SNR analsysis for lake vs dry ground at full-resolution for both VNIR and SWIR bands.

transmitted back out of the lake. All light coming from the lake floor that is reflected back down from the underside of the lake surface is assumed to never exit the lake.

Reflection and transmission off and into the lake is governed by the Fresnel equations, and illustrated below.

$$\rho_s = \left(\frac{n_1 \cos\theta - n_2 \sqrt{1 - \left(\frac{n_1}{n_2}\sin\theta\right)^2}}{n_1 \cos\theta + n_2 \sqrt{1 - \left(\frac{n_1}{n_2}\sin\theta\right)^2}} \right)^2 \quad (1)$$

$$\rho_p = \left(\frac{n_1 \sqrt{1 - \left(\frac{n_1}{n_2}\sin\theta\right)^2} - n_2 \cos\theta}{n_1 \sqrt{1 - \left(\frac{n_1}{n_2}\sin\theta\right)^2} + n_2 \cos\theta} \right)^2 \quad (2)$$

$$\rho = \frac{1}{2}\left(\rho_s(\theta, n_1, n_2) + \rho_p(\theta, n_1, n_2)\right) \quad (3)$$

where ρ_s and ρ_p are the specular and parallel surface reflectance, respectively. Furthermore, the angles of refraction are governed by Snell's law $n_1 \sin\theta_i = n_2 \sin\theta_t$ for incident angle θ_i and transmission angle θ_t:

$$\theta_r = \arcsin \frac{n_1}{n_2} \sin\theta \quad (4)$$

where θ_r is the refractive angle. The complex refractive index consists of a real part representing the index of refraction, and the imaginary part representing the extinction coefficient, or $n + i\kappa$ respectively. The attenuation of light due to extinction is expressed as $e^{\frac{-2\pi\kappa z}{\lambda_0}}$, where λ_0 is the vacuum wavelength. More simply, we use the coefficient $\alpha = \frac{2\pi\kappa}{\lambda_0}$. The values of α for liquid methane at 90K is obtained from [53]. The refractive index of liquid methane is assumed to be constant at $n = 1.288$. The Titan atmosphere is primarily nitrogen, with a refractive index of $n = 1.0002984$.

DISORT [32] is used to perform radiative transfer (RT) calculations to estimate the downwelling radiance L at the Titan surface. We assume a solar zenith of $45°$, lake depth of 5m, and a nadir pointed camera, and perform the RT calculations for the pixel centered in the camera's FOV.

Given a downwelling sky radiance map $L(\theta, \phi)$ at the Titan surface, we calculate a specular reflection map L_1 using the Fresnel equations above, and a downward radiance map L_2 at the lake floor that incorporates the refraction and attenuation into the lake. The irradiance E_2 at the lake floor is obtained by integrating the radiance over the hemisphere:

$$E_2 = \int_\phi \int_\theta L_2(\theta, \phi) \cos\theta \sin\theta d\theta d\phi + E_2^{direct} \quad (5)$$

Where E_2^{direct} is the direct solar radiant flux at the lake floor, taking into account the refraction, transmission, and attenuation mentioned above. Now, reflection off the lake floor is governed by Lambertian reflection; hence the upward radiance is calculated by:

$$\frac{\alpha_f E_2}{\pi} \quad (6)$$

Given the Lambertian assumption, the reflected radiance off the lake floor is uniform in all directions. The upward light is

again attenuated within the lake according to the path length, and refracted at the lake surface. The upwelling radiance map at the lake surface is designated L_3.

For estimating contrast ratios, two cases are considered where lake and dry ground, respectively. The RT calculations consider reflection off the ground, based on an input parameter for surface albedo. For the dry ground case, the albedo parameter above is used. For the lake case, an "effective albedo" is estimated by setting the RT albedo parameter to 0 and taking the ratio of our calculated upwelling light (angularly integrated) to the calculated downwelling + direct light at the surface. The RT calculation is then recomputed with this effective albedo to calculate the downwelling light with a Lambertian approximation of reflection for each wavelength.

We study the contrast ratios as a function of altitude. To estimate the light gathered at a given altitude y, the upwelling light at the surface is attenuated by incorporating the optical depth $\tau(dy)$ at each layer of the atmosphere model. Furthermore, to compute signal at the camera, weights designated as $w(dy)$ incorporate the geometry and efficiency of the sensor (as discussion in Sec 5). Signal is computed as:

$$S = L_3 \sum_y e^{\tau(dy)} w(dy) \tag{7}$$

The Contrast Signal-to-noise ratio is then estimated as:

$$SNR = \frac{S_{surface} - S_{lake}}{\sqrt{S_{surface}}\sqrt{2}} \tag{8}$$

Figure 9 shows the contrast SNR plot as a function of altitude for imagers in both the VNIR and SWIR spectral bands at megapixel resolution. The results shows we are are able to observe a favorable contrast SNR of $\sim$200, close to the ground; confirming our intuition that the methane lakes on Titan absorb most of the incident light, especially in the SWIR spetral band. Therefore, when viewed away from a reflection of the sun, the reflectivity contrast between lake and adjacent ground should allow us to discriminate these terrain types automatically in descent images. Furthermore, at lower resolution the contrast SNR numbers improve by the binning factor, b. Large contrast SNR values at map matching resolution thus facilitates onboard segmentation for map matching in the lake district.

In some dune fields, reflectance of interdune areas is higher than the dunes, which makes the interdunes appear brighter than dunes in imagery [37]. This is likely because in such areas the interdune regions have water ice content and are free of the darker sand composing the dunes. Since dune axes predominantly have an east-west orientation, the appearance of dune slopes facing away from the sun will be darkened further because of shading effects. These albedo and shading effects may combine to enable onboard dune vs interdune segmentation of descent imagery, which may enable steering descent systems toward landing on interdunes.

9. Multi-sensor State-Estimation

An extended Kalman filter for visual-inertial SLAM estimates the position, velocity, and orientation of the vehicle and the IMU gyro and accelerometer biases from 10 minutes before entry (E-10) until touchdown, fusing all of the measurements described earlier [17]. The filter was tested by itself using an end-to-end EDL simulator built for this project [54] to generate synthetic noisy measurements for the IMU and altimeter from E-10 to touchdown, for map matching from 40 to 20 km AGL, and for feature tracking from 20 km to touchdown. The noise model in the filter was tuned to be consistent with estimation errors on sample simulation trials.

Simulations processed five descent images per second, with one template match per image during map matching and 27 features as SLAM landmarks during feature tracking. Map matching operates for approximately one hour in the descent from 40 to 20 km and feature tracking operates for approximately 2.5 hours in the descent from 20 km to the surface. The position error covariance model in the filter converges to a 3σ value of less than 1 km at 20 km AGL for both the Huygens and Maracaibo sites. The 3σ uncertainty at touchdown is dominated by the feature tracking phase, which was modeled as operating in the same way for both test sites. As a result, the 3σ position uncertainty in the filter at touchdown was $\sim$ 2 km for both sites (Figure 10). These results depend on the modeled noise levels, which could change with further analysis, and a full error budget for precision landing includes other error sources [7]; nevertheless, these are promising results. More detailed discussion of the simulator and Monte Carlo simulation results is given in a companion paper [55].

10. Summary and Future Work

Titan's dense atmosphere, low gravity, and high winds at high altitudes create descent times of >90 minutes with standard EDL architectures and result in large unguided landing ellipses, with 99% values of $\sim$110x110 and 149x72 km in recent Titan lander proposals. Enabling precision landing on Titan could increase science return for the types of missions proposed to date and make additional types of landing sites accessible, opening up new possibilities for science investigations. Precision landing on Titan has unique challenges, because the hazy atmosphere makes it difficult to see the surface and because it requires guided descent with divert ranges that are one to two orders of magnitude larger than needed for other target bodies, i.e. up to on the order of 100 km. It is conceivable that such a divert capability could be provided economically by a parafoil or other steerable aerodynamic decelerator deployed several 10s of km above the surface. This would require a terrain relative navigation (TRN) capability that can operate at such altitudes, despite challenges of seeing the surface sufficiently clearly and of depending on map products that are two orders of magnitude lower in spatial resolution than those for Mars and airless bodies.

This paper addressed the TRN problem for Titan guided descent, assuming deployment of a parafoil at an altitude around 40 km. We defined a notional sensor suite including a navigation grade IMU, a radar altimeter, and two descent cameras, with spectral responses in the VNIR ($\sim$0.5 to 1 um) and SWIR ($\sim$2.0 to 2.1 um). Map resolutions of a few kilometers per pixel imply that traditional approaches to TRN that match descent images to prior maps are not applicable below a fairly high cut-off altitude, taken here to be roughly 20 km. This defines upper and lower altitude regimes in which different navigation techniques are required. TRN with map matching is applicable in the upper regime, but faces challenges caused by the hazy atmosphere. Parafoil descent from 20 km would take on the order of 2 hours,

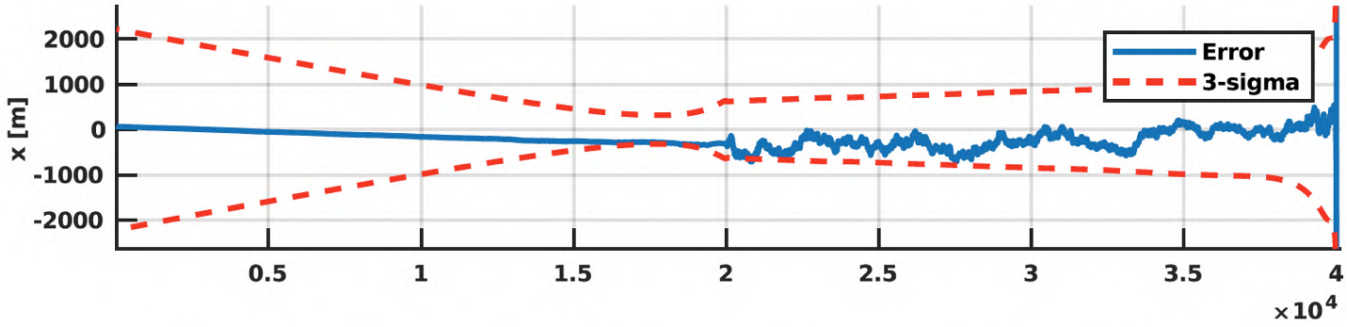

Figure 10. Simulated state estimation filter results for position, from 40 km AGL to the surface for the Huygens test site (both axes labeled in meters). The map matching error model represented the use of NCC to match simulated SWIR descent images to the ISS mosaic and the feature tracking error model was obtained from experiments with simulated descent images created from a Huygens DISR mosaic. Results for the Maracaibo Lacus test case (not shown) had a slightly lower 3 uncertainty in the map matching phase (40 to 20 km), due to using the higher resolution SAR mosaic for map matching, but approximately the same error at touchdown.

during which navigation using only an IMU and altimeter would accrue very large position error. Therefore, the lower altitude regime also requires some form of TRN to limit position error growth. Tracking features between descent images taken at different altitudes has potential to meet this need. At least two classes of landing site on Titan hold possibilities for a new approach, in which terrain types are recognized in descent images without reference to a prior map. These classes are lake districts and dune fields, where lake vs ground terrain types and dune vs interdune terrain types have reflectivity differences that may enable onboard image segmentation to automatically discriminate them. This might enable guidance and navigation relative to these zones all the way to the surface, regardless of limitations of prior reconnaissance imagery.

We established rough requirements for the contrast SNR (CSNR) of descent imagery needed to enable these functions by drawing on results from prior work with descent imagery from the Huygens probe and with stress testing of map matching algorithm for precision landing on Mars. The low resolution of map products actually helps to meet these requirements for map matching algorithms, because it leads to a substantial amount of binning of descent image pixels that improves SNR and reduces sensitivity to image smear caused by camera motion. For the upper altitude regime, where scattered light causes significant image contrast reduction, analysis showed that a SWIR descent camera should far exceed the CSNR requirements for map matching and have much better CSNR than a VNIR descent camera. In this regime, SWIR is the only option that may have sufficient CSNR for feature tracking. In the lower altitude regime, VNIR becomes better for feature tracking because contrast improves and much more light is available in that band.

We developed prototype map matching and feature tracking algorithms and tested them in case studies for two representative landing site scenarios: (1) the Huygens landing site, as a representative for any site where dry ground fills the landing ellipse, and (2) the Maracaibo Lacus interlake district, where small methane lakes are dispersed in the landing ellipse. For both cases, SWIR map mosaics from the Cassini VIMS instrument are available with sufficient resolution to create synthetic descent images for simulation-based algorithm testing. We used a radiative transfer model to produce appropriate levels of contrast and noise in these images, but did not model effects of camera optics. For the Huygens site, we tried using both a VNIR map mosaic and a synthetic aperture radar (SAR) mosaic. Since SAR and the simulated SWIR descent images have significantly different sensor phenomenology, we tried map matching methods based on mutual information. Initial results were not encouraging, so we then focused on experiments using the VNIR mosaic, sampled at 2 km/pixel. Template matching techniques obtained 3σ registration errors of $<$ 8 km in Monte Carlo simulations in the altitude range of 20 to 40 km. For the Maracaibo Lacus site, we noted that it should be possible to segment both the SAR mosaic and onboard SWIR descent images into lake vs non-lake pixels, which can convert this map matching problem into one of matching binary images. We tested this approach, again at 2 km/pixel, and obtained 3σ registration errors of $<$1.5 km.

For the lower altitude regime ($<$20 km AGL), feature detection and tracking algorithms were tested in Monte Carlo simulations where mosaics of descent imagery from the DISR instrument on the Huygens probe were used to create synthetic descent images. Results were promising, with RMS feature tracking errors $<$0.6 pixels. We also presented an image contrast analysis for lake districts that supports the possibility of automatic segmentation, though we did not develop or test algorithms for that.

An extended Kalman filter (EKF) was developed to fuse all of the sensor measurements to estimate position, velocity, attitude, and IMU bias states. This filter used simultaneous location and mapping (SLAM) techniques to include coordinates of tracked features in the state vector. Simulated sensor measurements were generated from E-10 to touchdown, with 5 Hz map matching updates from 40 to 20 km AGL and 5 Hz feature tracking updates from 20 km AGL to the surface. Filter process noise parameters were tuned to match initial Monte Carlo results from our simulator. Filtering many map matching measurements in the upper altitude regime converged filter error estimates to $<$1 km (3σ) at 20 km AGL for both landing site case studies. For the rest of the descent, simulated feature tracking was the same for both case studies, and the effect of feature tracking dominates error growth in the lower regime. As a result, the 3σ position error at touchdown modeled by the filter covariance matrix was around 2 km for both landing site case studies. These results are preliminary, based on initial measurement noise models and filter tuning, but they are quite promising.

Key directions for future work include enhancing the fidelity of the simulation-based testing process, including with higher fidelity models of descent cameras, and acquiring much larger data sets for testing. The latter probably requires acquiring analog data sets on Earth and/or creating virtual scene models for simulation. TRN for Titan will require a lot of onboard computation. Advanced flight computers with high computing throughput and very low size, weight, and power will be important for enabling this capability. Further maturation of this capability in the next decade has potential to make it available for missions in the 2030s. TRN methods for Titan could also have applicability to precision delivery of Titan balloons and navigation of Titan balloons after deployment. Guided descent on Venus may be of value for future Venus mission concepts; this would be even more difficult than on Titan due to more atmospheric scattering and the need to use radar mosaics as maps, but some of the methods used here are applicable to the Venus problem.

REFERENCES

[1] B. Kazeminejad, M. Pérez-Ayúcar, J.-P. Lebreton, M. Sanchez-Nogales, M. Belló-Mora, N. Strange, D. Roth, L. Popken, K. Clausen, and P. Couzin, "Simulation and analysis of the revised huygens probe entry and descent trajectory and radio link modelling," *Planetary and Space Science*, vol. 52, no. 9, pp. 799–814, 2004.

[2] R. D. Lorenz and C. E. Newman, "Twilight on ligeia: Implications of communications geometry and seasonal winds for exploring titans seas 2020–2040," *Advances in Space Research*, vol. 56, no. 1, pp. 190–204, 2015.

[3] M. J. Wright, J. A. Herath, H. H. Hwang, J. M. Corliss, A. M. Brandis, D. Buecher, D. Adams, and R. Lorenz, "The dragonfly entry and descent system," 2019.

[4] A. R. Hendrix, T. A. Hurford, L. M. Barge, M. T. Bland, J. S. Bowman, W. Brinckerhoff, B. J. Buratti, M. L. Cable, J. Castillo-Rogez, G. C. Collins *et al.*, "The nasa roadmap to ocean worlds," *Astrobiology*, vol. 19, no. 1, pp. 1–27, 2019.

[5] K. Stephan, R. Jaumann, E. Karkoschka, R. L. Kirk, J. W. Barnes, M. G. Tomasko, E. P. Turtle, L. Le Corre, M. Langhans, S. Le Mouélic *et al.*, "Mapping products of titan's surface," in *Titan from Cassini-Huygens*. Springer, 2009, pp. 489–510.

[6] E. Karkoschka, A. McEwen, J. Perry, and E. Turtle, "A global mosaic of titan's surface albedo using cassini images," in *AAS/Division for Planetary Sciences Meeting Abstracts*, vol. 50, 2018.

[7] A. Johnson, S. Aaron, J. Chang, Y. Cheng, J. Montgomery, S. Mohan, S. Schroeder, B. Tweddle, N. Trawny, and J. Zheng, "The lander vision system for mars 2020 entry descent and landing," 2017.

[8] M. San Martin, G. F. Mendeck, P. B. Brugarolas, G. Singh, F. Serricchio, S. W. Lee, E. C. Wong, and J. C. Essmiller, "In-flight experience of the mars science laboratory guidance, navigation, and control system for entry, descent, and landing," *CEAS Space Journal*, vol. 7, no. 2, pp. 119–142, 2015.

[9] S. Tavan, "Status and context of high altitude precision aerial delivery systems," in *AIAA Guidance, Navigation, and Control Conference and Exhibit*, 2006, p. 6793.

[10] R. Benney, A. Meloni, A. Cronk, and R. Tiaden, "Precision airdrop technology conference and demonstration 2007," in *20th AIAA Aerodynamic Decelerator Systems Technology Conference and Seminar*, 2009, p. 2927.

[11] T. Jann, "Advanced features for autonomous parafoil guidance, navigation and control," in *18th AIAA Aerodynamic Decelerator Systems Technology Conference and Seminar*, 2005, p. 1642.

[12] J.-P. Lebreton, O. Witasse, C. Sollazzo, T. Blancquaert, P. Couzin, A.-M. Schipper, J. B. Jones, D. L. Matson, L. I. Gurvits, D. H. Atkinson *et al.*, "An overview of the descent and landing of the huygens probe on titan," *Nature*, vol. 438, no. 7069, p. 758, 2005.

[13] J. R. Carr and J. S. Sobek, "Digital scene matching area correlator (dsmac)," in *Image Processing For Missile Guidance*, vol. 238. International Society for Optics and Photonics, 1980, pp. 36–41.

[14] G. B. Irani and J. P. Christ, "Image processing for tomahawk scene," *Johns Hopkins APL Technical Digest*, vol. 15, no. 3, pp. 250–264, 1994.

[15] A. R. Klumpp, "Pinpoint landing concepts for the mars rover sample return mission," in *Guidance and Control 1989*, 1989, pp. 423–432.

[16] S. Thurman, L. Matthies, J. Corliss, and R. K. Johnson, "Space flight test of vision-guided planetary landing system," in *AIAA Infotech@ Aerospace 2007 Conference and Exhibit*, 2007, p. 2767.

[17] A. I. Mourikis, N. Trawny, S. I. Roumeliotis, A. E. Johnson, A. Ansar, and L. Matthies, "Vision-aided inertial navigation for spacecraft entry, descent, and landing," *IEEE Transactions on Robotics*, vol. 25, no. 2, pp. 264–280, 2009.

[18] C. D. Epp, E. A. Robertson, and T. Brady, "Autonomous landing and hazard avoidance technology (alhat)," in *2008 IEEE Aerospace Conference*. IEEE, 2008, pp. 1–7.

[19] J. M. Carson, E. Robertson, N. Trawny, and F. Amzajerdian, "Flight testing alhat precision landing technologies integrated onboard the morpheus rocket vehicle," in *AIAA SPACE 2015 Conference and Exposition*, 2015, p. 4417.

[20] N. Trawny, A. Katake, Y. Cheng, D. Conway, M. San Martin, D. Skulsky, and A. E. Johnson, "The intelligent landing system for safe and precise landing on europa," 2017.

[21] A. Johnson, C. Bergh, Y. Cheng, D. Clouse, K. Gostelow, K. Ishikawa, A. Katake, K. Klaasen, M. Mandic, M. Morales *et al.*, "Design and ground test results for the lander vision system," in *36th Annual AAS Guidance and Control Conference*, 2013, pp. 13–042.

[22] "Airborne systems," https://airborne-sys.com/wp-content/uploads/2016/08/ASG_Hi5Canopy_20160830_mh.pdf.

[23] A. A. Wolf, C. Graves, R. Powell, and W. Johnson, "Systems for pinpoint landing at mars," 2004.

[24] E. Karkoschka and S. E. Schröder, "The disr imaging mosaic of titan's surface and its dependence on emission angle," *Icarus*, vol. 270, pp. 307–325, 2016.

[25] C. Nixon, R. Lorenz, R. Achterberg, A. Buch, P. Coll, R. Clark, R. Courtin, A. Hayes, L. Iess, R. Johnson *et al.*, "Titan's cold case files-outstanding questions after cassini-huygens," *Planetary and Space Science*, vol. 155, pp. 50–72, 2018.

[26] O. A. Yakimenko, *Precision aerial delivery systems: modeling, dynamics, and control*. American Institute of Aeronautics and Astronautics, Inc., 2015.

[27] G. Van der Kolf, "Flight control system for an autonomous parafoil," Ph.D. dissertation, Stellenbosch: Stellenbosch University, 2013.

[28] J. Underwood and R. Sinclair, "Windtunnel testing of parachutes for the huygens probe," *The Aeronautical Journal*, vol. 101, no. 1008, pp. 357–364, 1997.

[29] R. Trautner, H. Svedhem, J. Lebreton, N. Floury, D. Plettemeier, P. Couzin, N. Hughes, and P. Edenhofer, "Fmcw radars for entry probes and landers: Lessons learned from the huygens radar altimeter," *ESA SP*, vol. 607, 2005.

[30] M. G. Tomasko, D. Buchhauser, M. Bushroe, L. Dafoe, L. Doose, A. Eibl, C. Fellows, E. McFarlane, G. Prout, M. Pringle *et al.*, "The descent imager/spectral radiometer (disr) experiment on the huygens entry probe of titan," in *The Cassini-Huygens Mission*. Springer, 2003, pp. 469–551.

[31] S. Lingard, "Basic analysis of ram-air parachute," 2015.

[32] K. Stamnes, S.-C. Tsay, W. Wiscombe, and K. Jayaweera, "Numerically stable algorithm for discrete-ordinate-method radiative transfer in multiple scattering and emitting layered media," *Applied optics*, vol. 27, no. 12, pp. 2502–2509, 1988.

[33] L. R. Doose, E. Karkoschka, M. G. Tomasko, and C. M. Anderson, "Vertical structure and optical properties of titans aerosols from radiance measurements made inside and outside the atmosphere," *Icarus*, vol. 270, pp. 355–375, 2016.

[34] E. Karkoschka and M. G. Tomasko, "Methane absorption coefficients for the jovian planets from laboratory, huygens, and hst data," *Icarus*, vol. 205, no. 2, pp. 674–694, 2010.

[35] J. W. Barnes, L. Lemke, R. Foch, C. P. McKay, R. A. Beyer, J. Radebaugh, D. H. Atkinson, R. D. Lorenz, S. Le Mouélic, S. Rodriguez *et al.*, "Aviatraerial vehicle for in-situ and airborne titan reconnaissance," *Experimental Astronomy*, vol. 33, no. 1, pp. 55–127, 2012.

[36] E. Karkoschka and S. E. Schröder, "Eight-color maps of titans surface from spectroscopy with huygens disr," *Icarus*, vol. 270, pp. 260–271, 2016.

[37] L. E. Bonnefoy, A. G. Hayes, P. O. Hayne, M. J. Malaska, A. Le Gall, A. Solomonidou, and A. Lucas, "Compositional and spatial variations in titan dune and interdune regions from cassini vims and radar," *Icarus*, vol. 270, pp. 222–237, 2016.

[38] L. G. Brown, "A survey of image registration techniques," *ACM computing surveys (CSUR)*, vol. 24, no. 4, pp. 325–376, 1992.

[39] B. Zitova and J. Flusser, "Image registration methods: a survey," *Image and vision computing*, vol. 21, no. 11, pp. 977–1000, 2003.

[40] S. Krig, "Interest point detector and feature descriptor survey," in *Computer vision metrics*. Springer, 2016, pp. 187–246.

[41] A. Ansar and L. Matthies, "Multi-modal image registration for localization in titan's atmosphere," in *2009 IEEE/RSJ International Conference on Intelligent Robots and Systems*. IEEE, 2009, pp. 3349–3354.

[42] L. Matthies, B. Rothrock, S. Daftry, A. Davis, and M. Malaska, "Map matching during descent for terrain relative navigation on titan," in *International Planetary Probe Workshop (IPPW)*, 2019.

[43] C. F. Olson, "Maximum-likelihood template matching," in *Proceedings IEEE Conference on Computer Vision and Pattern Recognition. CVPR 2000 (Cat. No. PR00662)*, vol. 2. IEEE, 2000, pp. 52–57.

[44] R. Brunelli, *Template matching techniques in computer vision: theory and practice*. John Wiley & Sons, 2009.

[45] J. N. Maki, C. M. McKinney, R. G. Sellar, R. G. Willson, D. S. Copley-Woods, D. C. Gruel, D. L. Nuding, M. Valvo, T. Goodsall, J. McGuire, J. Kempenaar, and T. E. Litwin, "Enhanced engineering cameras (eecams) for the mars 2020 rover," in *3rd International Workshop on Instrumentation for Planetary Missions*, vol. 1980, 2016.

[46] H. U. Keller, B. Grieger, M. Küppers, S. E. Schröder, Y. V. Skorov, and M. G. Tomasko, "The properties of titan's surface at the huygens landing site from disr observations," *Planetary and Space Science*, vol. 56, pp. 728–752, 2008.

[47] E. Karkoschka, M. G. Tomasko, L. R. Doose, C. See, E. A. McFarlane, S. E. Schröder, and B. Rizk, "Disr imaging and the geometry of the descent of the huygens probe within titan's atmosphere," *Planetary and Space Science*, vol. 55, pp. 1896–1935, 2007.

[48] E. Rosten and T. Drummond, "Fusing points and lines for high performance tracking," in *2005 IEEE International Conference on Computer Vision*. IEEE, October 2005, pp. 1508–1511.

[49] B. D. Lucas and T. Kanade, "An iterative image registration technique with an application to stereo vision," in *7th International Joint Conference on Artificial Intelligence*, April 1981, pp. 674–679.

[50] C. Tomasi and T. Kanade, "Detection and tracking of point features," Carnegie Mellon University, Tech. Rep., April 1991.

[51] J. Shi and C. Tomasi, "Good features to track," in *1994 IEEE Conference on Computer Vision and Pattern Recognition*. IEEE, 1994, pp. 593–600.

[52] P. H. S. Torr and A. Zisserman, "Mlesac: A new robust estimator with application to estimating image geometry," *Computer Vision and Image Understanding*, vol. 78, pp. 138–156, 2000.

[53] J. V. Martonchik and G. S. Orton, "Optical constants of liquid and solid methane," *Applied optics*, vol. 33, no. 36, pp. 8306–8317, 1994.

[54] M. B. Quadrelli, A. Schutte, J. Rimani, and L. Ermolli, "Aero maneuvering dynamics and control for precision landing on titan," in *IEEE Aerospace Conference*, 2019.

[55] A. Schutte, J. Delaune, E. Sklyanskiy, R. Hewitt, S. Daftry, M. B. Quadrelli, and L. Matthies, "Integrated simulation and state estimation for precision landing on titan," in *IEEE Aerospace Conference*, 2020.

BIOGRAPHY

Larry Matthies *is a Senior Research Scientist at the Jet Propulsion Laboratory. He has conducted research there on computer vision-based autonomous navigation of robotic vehicles for 30 years. He defined initial versions of several vision algorithms that have been used on Mars or are their way to Mars for the 2020 mission, including stereo vision and visual odometry for rover navigation, feature tracking for velocity estimation during terminal descent in the Descent Image Motion Estimation System for the MER mission, and terrain relative navigation for Mars precision landing, which is now built into the 2020 Mars landing system. He has also been a Principal Investigator in many autonomous navigation research programs funded by DARPA and the U.S. Army. He obtained his PhD in computer science from Carnegie Mellon University in 1989 and is a Fellow of the IEEE.*

Shreyansh Daftry *is a Robotics Technologist at NASA Jet Propulsion Laboratory, California Institute of Technology. He received his M.S. degree in Robotics from Carnegie Mellon University, and his B.S. degree in Electronics and Communication Engineering in 2013. His research interests lies at the intersection of space technology and autonomous robotic systems, with an emphasis on computer vision and machine learning. At JPL, he works on mission formulation for Mars Sample Return, and technology development for autonomous navigation of ground, airborne and subterranean robots.*

Brandon Rothrock *is a former member of the computer vision group at JPL. His research is focused on models for semantic image understanding, visual perception and obstacle avoidance for micro UAVs, and object detection. In September 2019, he joined Paige, where he is applying machine learning methods to medical image analyses. Brandon obtained his Ph.D. in Computer Science from UCLA, and a B.S. in Aeronautics and Astronautics from the University of Washington.*

Anthony B. Davis *holds a BSc in Physics & Astrophysics from U. Pierre & Marie Curie (1977), a MS in Physics & Astronomy from U. de Montréal (1981), and a PhD in Physics from McGill U. (1992). He has been working for over 25 years on innovative methods in cloud remote sensing from ground-, aircraft- and space-based platforms, as well as on the related problem of how clouds impact the Earths energy and hydrological cycles. He has held positions successively at NASA Goddard Space Flight Center in Greenbelt, Maryland, DOEs Los Alamos National Laboratory in New Mexico, and now at NASA's Jet Propulsion Laboratory in Pasadena, Ca. He specializes in the challenges posed by the 3D shapes and internal structures of real clouds to which he brings to bear his expertise in theoretical and computational radiative transfer in application to physics-based modeling and exploitation of the spatial, directional, spectral and/or polarimetric signals from clouds.*

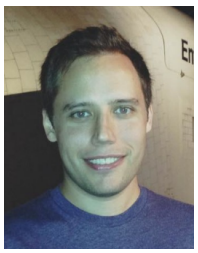

Robert Hewitt *received his Ph.D. degree in Electrical and Computer Engineering in 2018 from Queen's University (Kingston, Canada), after a M.A.Sc. in Aerospace Engienering from Carleton University (Ottawa, Canada) and a B.A.Sc in Engineering Physics from the University of Saskatchewan (Saskatoon, Canada). He is currently a post-doctoral research scientist at the Jet Propulsion Laboratory. He develops autonomous navigation systems for aerial and ground vehicles used in prospective planetary missions. His interests include state estimation, perception, and instrumentation.*

Evginey Sklyanskiy *received a B.S. in Aerospace Engineering from University of Illinois at Urbana-Champaign (UIUC). He continued the graduate studies at UIUC, and acquired a M.S. in Applied Mathematics and Aerospace Engineering. In the year of 2004, Evgeniy joined JPL and was working on low thrust trajectory optimization problems in the Mission Design and Navigation (MDNAV) section under the Outer Planetary group. Later in the career, the author has joined the EDL Guidance and Control Systems Group, where he has worked on Hayabusa/MUSES-C comet sample return mission, MSL surface operations and InSight MDNAV/EDL targeting analysis.*

Jeff Delaune *received his Ph.D. in Robotics from Institut Supérieur de l'Aéronautique et de l'Espace (ISAE, France) in 2013, after a M.S. in Astronautics and Space Engineering from Cranfield University (United Kingdom), and a B.S./M.S. in Engineering from École Centrale de Nantes (France). He is currently a robotics technologist at the Jet Propulsion Laboratory. He develops autonomous navigation systems for planetary exploration, with a focus on flying vehicles. Jeff was part of the navigation team for NASA's Mars Helicopter flight project. His interests include state estimation, sensor fusion, perception and computer vision.*

Aaron Schutte *is a Robotics Systems Engineer in the Modeling and Simulation Group at NASA JPL where he supports the development of advanced high-fidelity multi-mission simulation tools in the DARTS Lab. Prior to joining JPL he worked as a researcher in the Vehicle Systems Division at The Aerospace Corporation developing computational tools and algorithms for analysis of spacecraft GN&C systems and GPS. His primary contributions are in the development of high fidelity rigid and flexible multibody simulations, spacecraft control design and estimation techniques, and development of automatic derivative methods. He is a Senior Member of the AIAA and has served as a regular member of the AIAA GN&C Technical Committee.*

Joshua Yurtsever *is a senior computer science major at UC Berkeley and is interested in computer vision, computational photography, and optics. Josh has worked in NASA JPLs Computer Vision Group, Facebook Data Science, and the UC Berkeley Computational Imaging Lab. With a background in physics as well as computer science, Josh has a strong passion for research and hopes to pursue a PhD after graduation. In his spare time, Josh likes to play the pipe organ and ride his bike.*

Michael Malaska *is a scientist in the Planetary Ices Group at NASA/JPL. He obtained his undergraduate degree in chemistry from MIT, his PhD in chemistry from UC Berkeley, and performed postdoctoral research in neurochemistry at Mayo Clinic Jacksonville in Florida. After a 20 year career in the pharmaceutical industry inventing new medicines, images of Titans alien surface sent down by the Cassini spacecraft ignited his passion in planetary science. He went from being an interested amateur, to a volunteer researcher, and ultimately changed his career to planetary science and astrobiology. His current research program combines laboratory simulation, spacecraft remote sensing, and field geology to explore and understand Saturns moon Titan. He has done field work in North Carolina, the Mojave Desert and Salton Sea in California, the Greenland Ice Sheet, and an extremophile sulfide cave in southern Mexico.*